

- (13) Murray, C. T.; Gilmer, J. W.; Stein, R. S. *Macromolecules* 1985, 18, 996.
- (14) Bates, F. S.; Wignall, G. D. *Macromolecules* 1986, 19, 934.
- (15) Binder, K. *J. Chem. Phys.* 1983, 79, 6387.
- (16) Kramer, E. J.; Green, P. F.; Palmström, C. J. *Polymer* 1984, 25, 473.
- (17) Sillescu, H. *Makromol Chem., Rapid Commun.* 1984, 5, 519.
- (18) Composto, R. J.; Mayer, J. W.; Kramer, E. J.; White, D. M. *Phys. Rev. Lett.* 1986, 57, 1312.
- (19) Jones, R. A. L.; Klein, J.; Donald, A. M. *Nature (London)* 1986, 321, 161.
- (20) Composto, R. J.; Kramer, E. J.; White, D. M. *Nature (London)* 1987, 323, 1980.
- (21) Sillescu, H. *Makromol. Chem., Rapid Commun.* 1987, 8, 393.
- (22) Composto, R. J. Ph.D. Thesis, Cornell University, 1987, pp 94-130.
- (23) Composto, R. J.; Kramer, E. J.; White, D. M. *Macromolecules* 1988, 21, 2580.
- (24) Kirste, R. G., personal communication.
- (25) Murschall, U.; Fischer, E. W.; Herkt-Maetzky, Ch.; Fytas, G. *J. J. Polym. Sci., Polym. Lett. Ed.* 1986, 24, 191.
- (26) Strobl, G. R.; Urban, G. *Colloid Polym. Sci.*, in press.

Small-Angle Neutron Scattering from a Bisphenol A Carbonate/Dimethylsiloxane Copolymer under Uniaxial External Stretch

B. Hammouda* and W. B. Yelon

Research Reactor Facility and Department of Physics, The University of Missouri, Columbia, Missouri 65211

A. C. Lind

McDonnell Douglas Research Labs, St Louis, Missouri 63166

F. Y. Hansen

Fysisk-Kemisk Institut, The Technical University of Denmark, 206 DTH DK 2800 Lyngby, Denmark. Received July 29, 1987; Revised Manuscript Received April 22, 1988

ABSTRACT: There is previous evidence that random copolymers of bisphenol A carbonate (BPAC) and dimethylsiloxane (DMS) form microdomain morphology. Small-angle neutron scattering (SANS) is used to investigate this system, which shows a broad-peak spectrum. The origin of this peak is due to interference scattering between the BPAC-rich microdomain and the DMS-rich interdomain regions. SANS measurements taken from such a random copolymer (50%/50% mixture) under uniaxial external stretch show that the glassy microdomains do not follow the external drawing whereas the rubbery interdomain regions do. Two data analysis methods are used: one based on nonlinear least-squares fits of the raw data to a model consisting of two confocal ellipsoids representing the deformed microdomain morphology and the other on a two-dimensional Fourier transform of SANS data to obtain an anisotropic pair correlation function.

Introduction

Small-angle (neutron or X-ray) scattering is well suited to investigate the morphology of copolymer systems. This technique, when supplemented with some theoretical analysis, has been successfully applied to a number of copolymer systems in the solid¹⁻⁶ or melt⁷⁻⁸ forms. For instance, SANS from either of these phases shows a broad-peak spectrum. The origin of this peaked behavior, however, is different. In the case of solid block copolymers, the peak is due to interference scattering between microdomain and interdomain regions (microphase segregation) while in block copolymer melts, it is due to a correlation hole⁹ around single blocks, i.e., the probability of finding in the vicinity of a monomer another similar monomer belonging to a different block is decreased due to the repulsion of the polymer coils that is required to ensure the incompressibility of the system. In the Porod range, the former case shows a $1/Q^4$ decay (Q being the scattering wavenumber) while the latter case presents a $1/Q^2$ decrease characterizing correlations in Gaussian chains.

The solid randomly alternating copolymer of bisphenol A carbonate and dimethylsiloxane¹⁰ (50%/50% random mixture of BPAC and DMS) investigated in this paper shows a broad SANS peak around $Q = 0.05 \text{ \AA}^{-1}$ with no higher harmonic peaks. The origin of this single peak is discussed. The effect of a uniaxial external stretch on microdomain morphology is also discussed by using two methods: one based on a nonlinear least-squares fit of the

two-dimensional (2D) raw data and another method based on a 2D Fourier transform of SANS data. It should be noted that the experiments reported here do not take full advantage of the SANS technique because no deuteriated samples are used. SANS can, however, be used interchangeably with SAXS on phase-segregated samples. In fact, SAXS data have been taken^{11,12} on BPAC/DMS block copolymers and can be seen to qualitatively agree with SANS data. The purpose of the present investigations is to study the stretched morphology.

SANS Measurements and Data Analysis

SANS measurements are taken on a well characterized BPAC/DMS random copolymer sample unstretched and under uniaxial external stretch.

Sample Preparation and Characterization. The BPAC/DMS sample used in this study was obtained from H. A. Vaughn.¹³ This sample contains 50 wt % BPAC. The block lengths are polydisperse, having a number-average degree of polymerization of about 6 for the BPAC blocks and about 20 for the DMS blocks. Additional sample characterization data have been reported previously.^{14,15} For this composition and block lengths, the BPAC blocks associate into rigid domains joined together by the rubbery DMS blocks. NMR¹⁶ results support a proposed spherical BPAC domain morphology in which the longest blocks reside at the center and the shortest blocks reside at the surface, with a gradation of block

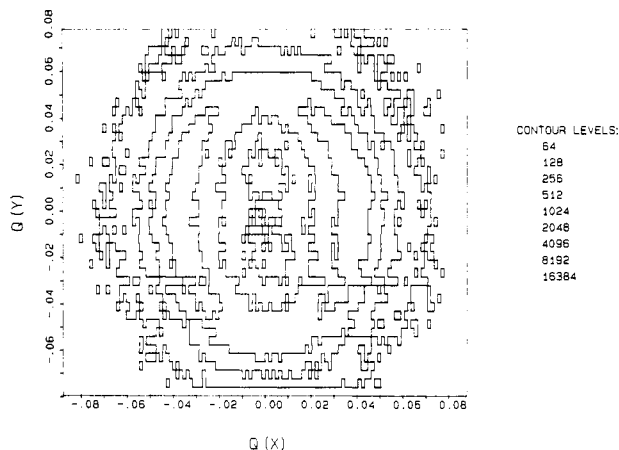


Figure 1. Two-dimensional isointensity contour map for the BPAC/DMS copolymer sample stretched to an extension ratio of 1.24.

lengths in between. Note that at this composition, regular (nonrandom) block copolymers form a lamellar morphology.

The BPAC/DMS sample for SANS study was prepared from 10% methylene chloride solutions. The solution was poured into a 68-mm diameter glass cylinder placed on a level, stretched cellophane film. Cardboard was placed on the top, and the methylene chloride was allowed to slowly evaporate over a period of 5 days. The cast films were pulled free of the cellophane and dried in a vacuum oven at 390 K for 48 h.

SANS Measurements. A piece of the BPAC/DMS sample (3 cm × 2 cm × 1 mm) was mounted on a stretching device consisting of a vise with a movable arm. The strain was read off a graduation on the fixed frame. SANS measurements have been performed with the University of Missouri Research Reactor SANS instrument¹⁷ using the following configuration: neutron wavelength of 4.75 Å (4% wavelength resolution), sample-to-detector matched path distance of 4.50 m, source and sample apertures of 2 and 1 cm, respectively, yielding a detector resolution of 0.004 Å⁻¹. Because of the fact that the two-dimensional area detector is an array of 43 (1/2 in. thick) position-sensitive detectors, the resolution along the detectors (in the X direction) is 2.5 times better than that in the direction perpendicular to them. In this typical instrument configuration, the accessible Q range is 0.008 Å⁻¹ < Q < 0.09 Å⁻¹.

Intensity data were collected in 8-h runs from unstrained and strained samples. The strain was applied in the X direction, and four different extensions were investigated. A beam open background was then subtracted from each one of these runs. The isointensity contours (Figure 1) are highly asymmetric (except for the unstrained case) so that the usual radial averaging method is inappropriate except for the unstrained sample. These isointensity maps are seen to follow elliptical shapes; however, the eccentricity of these ellipses is highly Q dependent as shown in Table I (i.e., ellipses are more elongated close to the center of the detector plane), which rules out the elliptical averaging technique (that proved useful in other instances¹⁸) as well. Because no straightforward averaging technique is available, SANS raw data corresponding to the stretched cases are either directly fitted to a model or Fourier transformed to give a two-dimensional pair correlation function.

Two-Dimensional Fourier Transforms of SANS Raw Data from Stretched BPAC/DMS. The Fourier transform of the structure factor $S(Q)$ (which is shown in Figure 2) is the pair correlation function $G(r)$, which dis-

Table I
Eccentricities and Orientation Angles (Degrees) of the Different Isointensity Contour Maps Fitted (Nonlinear Least-Squares Fit to Confocal Ellipses) in Various Q Ranges^a

run name	ext draw ratio	Q range of the fit, Å ⁻¹			
		0.01, 0.02	0.02, 0.03	0.03, 0.04	0.04, 0.05
CPNS	1.00	1.00	1.00	1.00	1.00
CPS1	1.12	0.62, 88	0.70, 90	0.76, 84	0.88, 80
CPS2	1.24	0.50, 88	0.58, 86	0.70, 88	0.82, 82
CPS3	1.35	0.43, 88	0.52, 88	0.68, 82	0.82, 86
CPS4	1.47	0.36, 88	0.38, 88	0.66, 82	0.74, 86

^aThe extension draw ratio corresponds to the ratio of the sample lengths after stretching to before stretching.

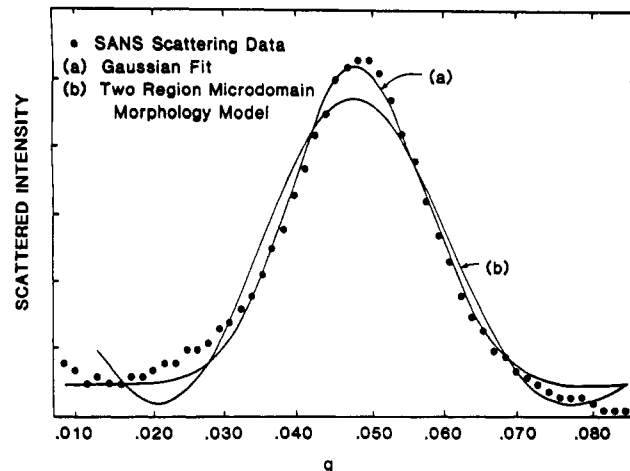


Figure 2. SANS data from unstretched BPAC/DMS: (a) fit to a Gaussian form for $S(Q)$; (b) fit to a two-region microdomain morphology model.

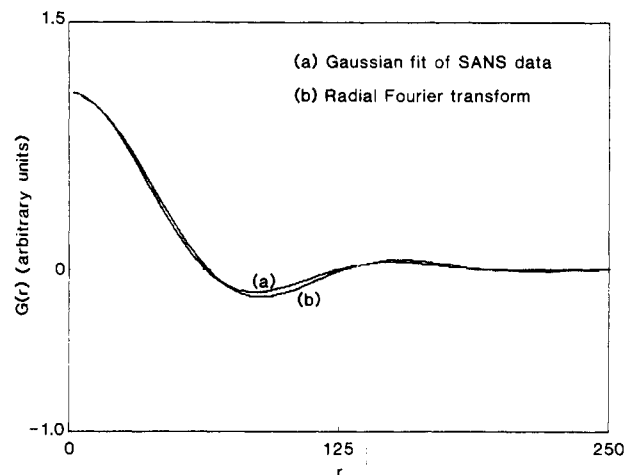


Figure 3. Radial pair correlation function $G(r)$ obtained as (a) the Fourier transform of a Gaussian $S(Q)$ and (b) the Fourier transform of SANS data from the unstretched BPAC/DMS sample.

plays an oscillatory damped behavior (Figure 3). The first oscillation is essential to observe the interference peak in $S(Q)$ and yields an average effective microdomain size (first zero of $G(r)$) and interdistance (distance to the first maximum of $G(r)$). It should be mentioned that choosing the first zero of $G(r)$ to represent an average (i.e., effective) microdomain size is not strictly correct. The microdomain size should be determined by the first zero of the average density fluctuation and not the pair correlation function. The effective size obtained for $G(r) = 0$ is reported for qualitative purposes only.

Table II
Variation of Microdomains Absolute (Angstroms) and Relative Sizes and Interdistances with the Extension Ratio along (Columns 3 and 4) and Perpendicular to (Columns 5 and 6) the Stretch Direction^a

case	ext ratio	$G(0,r_{\parallel})$ abs, rel eff sizes parallel to the stretch axis		$G(r_{\perp},0)$ abs, rel eff sizes perpendicular to the stretch axis	
		microdomain	interdomain	microdomain	interdomain
CPNS	1.0	61, 1.00 (0.07)	147, 1.00 (0.03)	65, 1.00 (0.06)	147, 1.00 (0.03)
CPS1	1.12	61, 1.00 (0.07)	168, 1.14 (0.02)	65, 1.00 (0.06)	139, 0.94 (0.03)
CPS2	1.24	65, 1.07 (0.06)	180, 1.22 (0.02)	69, 1.06 (0.06)	135, 0.92 (0.03)
CPS3	1.35	65, 1.07 (0.06)	192, 1.31 (0.02)	69, 1.06 (0.06)	131, 0.89 (0.03)
CPS4	1.47	69, 1.13 (0.06)	205, 1.39 (0.02)	69, 1.06 (0.06)	131, 0.89 (0.03)

^aMicrodomain sizes and interdistances are obtained from the first zero and first maximum of $G(r_{\perp},r_{\parallel})$, respectively. Numbers in parentheses are uncertainties based on the 4-Å uncertainty on the microdomain sizes and interdomain distances.

In the stretched sample cases, no directional averaging of the data is available since the radial and elliptical averaging techniques are inappropriate. One of the alternatives is to Fourier transform the two-dimensional raw (nonaveraged) data back to configuration space. There are two ways of doing that: through either a cartesian or a cylindrical two-dimensional Fourier transform.

In the case of a Fourier transform in cylindrical coordinates, anisotropic inhomogeneities in the sample are assumed to be cylindrically symmetric. This is, in general, the case for stretched samples where both directions perpendicular to the stretch axis are equivalent. A pair correlation function can be obtained:

$$G(r_{\perp},r_{\parallel}) = \int_0^{\infty} dQ_{\perp} Q_{\perp} \int_0^{2\pi} d\phi \int_{-\infty}^{\infty} dQ_{\parallel} \times \exp(iQ_{\perp}r_{\perp} \cos \phi + iQ_{\parallel}r_{\parallel})S(Q_{\perp},Q_{\parallel}) = \int_0^{\infty} dQ_{\perp} Q_{\perp} \int_0^{\infty} dQ_{\parallel} J_0(Q_{\perp}r_{\perp}) \cos(Q_{\parallel}r_{\parallel})S(Q_{\perp},Q_{\parallel})$$

where \perp and \parallel are directions perpendicular and parallel to the stretch axis (which is along the one-dimensional detectors in our case), $J_0(x)$ is the cylindrical Bessel function of order zero and $S(Q_{\perp},Q_{\parallel})$ is the raw SANS data corrected for incoherent background. Since this pair correlation function is numerically normalized to $G(0,0) = 1$, constant terms such as π entering in the definition of $J_0(x)$ have not been included. Table II contains a listing of the first zeros and first maxima of $G(r_{\perp},r_{\parallel})$ in both directions. These represent average microdomain effective sizes and interdistances, respectively. We have also included ratios of these values for the stretched and unstretched cases. As noted before, the first zero of $G(r_{\perp},r_{\parallel})$ does not correspond precisely to the edge of the microdomain, but it is used to define an effective size for it.

Table II shows that microdomain sizes do not vary in both directions whereas interdomain distances follow the external stretching fairly well in the parallel direction. This conclusion applies to all cases (to within the 4-Å uncertainty) except for the last one (extension ratio of 1.47), which may not be reliable (nonlinear effects such as stress relaxation start contributing significantly). The average microdomain volume does not change, whereas an average volume that includes interdomain regions increases only be 3% (compare $3.18 \times 10^6 \text{ \AA}^3$ before stretching to $3.29 \times 10^6 \text{ \AA}^3$ for a relative external stretch of 1.35). This means that the amount of free volume in the DMS-rich regions is not considerably increased upon stretching: the 3% increase is too small to be definitely qualified as a real effect and may be due to experimental uncertainties.

Least-Squares Fit to a Two-Region Ellipsoidal Microdomain Morphology. On the basis of the pair correlation function profile discussed above, a simple microdomain model¹⁹ consisting of an inner core of en-

Table III
Least-Squares Fit of SANS Raw Data to a Two-Region Ellipsoidal Microdomain Model

	ext	eff sizes			
		parallel to the stretch axis, Å		perpendicular to the stretch axis, Å	
		micro-domain ^a	inter-domain ^b	micro-domain ^a	inter-domain ^b
CPNS	1.0	64	152	64	153
CPS1	1.12	60	174	56	148
CPS2	1.24	61	188	55	146
CPS3	1.35	67	200	56	143
CPS4	1.47	63	212	52	137

^aMicrodomain sizes are obtained as the quantities a_1 along the stretch axis and $a_{1\epsilon_1}$ perpendicular to it. ^bInterdomain (center-to-center) distances are obtained as the quantities $a_1 + a_2$ along the stretch axis and $a_{1\epsilon_1} + a_{2\epsilon_2}$ perpendicular to it.

hanced scattering density and an outer layer of less scattering density with respect to the average scattering density of the sample is considered. Outside these regions, the scattering density is assumed to be uniform and equal to the average scattering density of the sample. Starting at the center of a microdomain and going radially outward, the inner core corresponds to the BPAC-rich microdomain itself, the outer depleted density region corresponds to the DMS-rich region (containing a small number of dispersed BPA blocks) surrounding that microdomain, and the constant density background corresponds to the annularly averaged (intra- and interdomain) density including and beyond the neighboring microdomains. This picture is an average over the whole sample. This model is reminiscent of a disordered lattice. A number of other liquidlike models (micellar model, zone model, and molecular dumbbell model) have been introduced¹² to describe BPAC/DMS block copolymer systems.

Upon stretching, the two-region spherical microdomain morphology is expected to become an ellipsoidal morphology with inner and outer ellipsoids of revolution of different eccentricities ϵ_1 and ϵ_2 . A structure factor for this model is available and has been used to fit the raw data corrected for background:

$$S(Q) = [C_1 3j_1(Q_1 a_1) / Q_1 a_1 - C_2 3j_1(Q_2 a_2) / Q_2 a_2]^2$$

where

$$Q_{1,2} = (Q_{\parallel}^2 + \epsilon_{1,2}^2 Q_{\perp}^2)^{1/2}$$

and a_1 and a_2 represent the major axes of the ellipsoids. These parameters (C_1 , a_1 , ϵ_1 , C_2 , a_2 , ϵ_2) along with a Q -independent background are extracted by performing a nonlinear least-squares fit of the SANS raw data (Figure 4). As Table III shows, microdomains do not seem to change upon stretching in the parallel direction. In the perpendicular direction, the small changes may be an artifact due to the large number (seven) of fitting parameters.

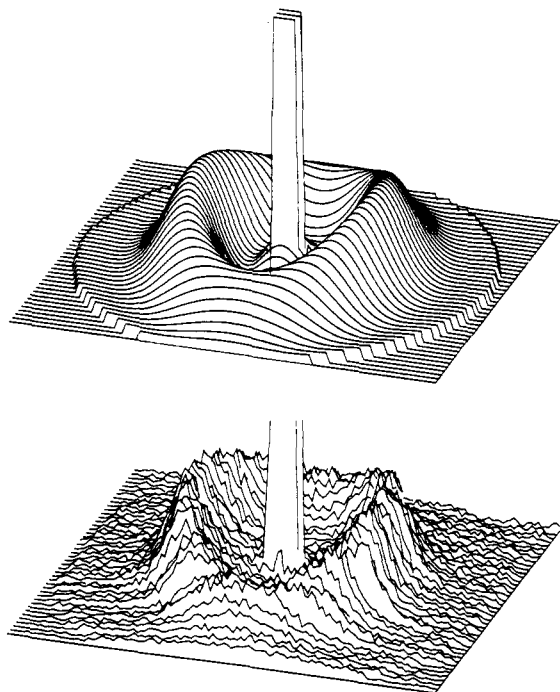


Figure 4. SANS raw data for the BPAC/DMS stretched to 1.24 extension ratio fitted to a two-ellipsoidal microdomain morphology model.

Interdomain distances on the other hand increase substantially in the parallel direction and shrink in the perpendicular direction. These fits show reasonable qualitative trends that agree with the results shown in Table II.

Discussion and Conclusions

SANS from a BPAC/DMS sample shows one broad peak which is due to interference scattering between the inner microdomain core and the outer interdomain regions. Two routes are possible to analyze scattering data from such amorphous systems: one can either Fourier transform the data back to configuration space to obtain a pair correlation function or devise some model to describe the inhomogeneities that are creating a contrast to the probing radiation and fit the data to the calculated scattering function. Both routes have been followed for both the unstretched and stretched BPAC/DMS cases. Pair correlations are seen to decrease to zero at large distances but through oscillations. The negative portion of $G(r)$ is necessary to obtain a SANS peaked spectrum. A simple model based on spherical microdomains is used. Evidence for this model has been presented by Niznik and Legrand¹⁵ and Lind.¹⁶ Electron micrographs from BPAC/DMS random copolymer systems have been taken by Tang.²⁰

When the external stretching is applied, microdomain sizes do not change, whereas interdomain regions are elongated along the stretch direction. These conclusions

are based on both a nonlinear least-squares fit to the 2D data and on a Fourier transform of the raw data in cylindrical coordinates. The nonlinear least-squares fits of the 2D data to the two-ellipsoidal model show that the eccentricity of the inner ellipsoid ϵ_1 does not change much compared to the eccentricity ϵ_2 of the outer one. A three-region ellipsoidal model would fit the data better but cannot be trusted because of the large number (nine) of fitting parameters. A Fourier transform of the raw data in cartesian coordinates can be misleading, because it results in an integrated pair correlation whose shape, zeros, and maxima are different from those of the pair correlation itself. For instance, a Fourier transform of SANS intensity data corresponding to one-dimensional detector sectors along and perpendicular to the stretch directions looks different from one-dimensional radial Fourier transform. Fitting of such intensity data sectors to reasonable functional forms (as is commonly done^{21,22}) is, however, a proper procedure to follow.

Acknowledgment. This research has been supported under the McDonnell Douglas Independent Research and Development Program. A discussion with Prof. P. W. Schmidt and Dr. H. Kaiser's help with the SANS instrument are greatly appreciated. F.Y.H. thanks the Danish Natural Science Foundation for financial support.

Registry No. Neutron, 12586-31-1.

References and Notes

- (1) Hadziioannou, G.; Skoulios, A. *Macromolecules* **1982**, *15*, 267.
- (2) Koberstein, J. T.; Stein, R. S. *J. Polym. Sci., Polym. Phys. Ed.* **1983**, *21*, 1439; **1983**, *21*, 2181.
- (3) Richards, R. W.; Thomason, J. L. *Macromolecules* **1983**, *16*, 982.
- (4) Bates, F. S.; Berney, C. V.; Cohen, R. E.; Wignall, G. D. *Polymer* **1983**, *24*, 519.
- (5) Miller, J. A.; Cooper, S. I.; Han, C. C.; Pruckmayr, G. *Macromolecules* **1984**, *17*, 1063.
- (6) Hasegawa, H.; Hashimoto, J.; Kawai, H.; Lodge, T. P.; Amis, E. J.; Glinka, C. J.; Han, C. C. *Macromolecules* **1985**, *18*, 67.
- (7) Leibler, L. *Macromolecules* **1980**, *13*, 1602.
- (8) Bates, F. S. *Macromolecules* **1985**, *18*, 525.
- (9) de Gennes, P.-G. *Scaling Concepts in Polymer Physics*; Cornell University Press: Ithaca NY, 1979.
- (10) LeGrand, D. G. *J. Polym. Sci. B* **1969**, *7*, 579.
- (11) LeGrand, D. G. *Polym. Lett.* **1970**, *8*, 195.
- (12) Legrand, A. D.; Vitale, D. G.; LeGrand, D. G. *Polym. Eng. Sci.* **1977**, *17*, 598.
- (13) Vaughn, H. A. *J. Polym. Sci. B* **1969**, *7*, 569.
- (14) Kambour, R. P. *J. Polym. Sci. B* **1969**, *7*, 573.
- (15) Niznik, G. E.; Legrand, D. G. *J. Polym. Sci., Polym. Symp.* **1977**, *60*, 97.
- (16) Lind, A. C. *Macromolecules* **1984**, *17*, 300.
- (17) Mildner, D. F. R.; Berliner, R.; Pringle, O. A.; King, J. S. *J. Appl. Crystallogr.* **1981**, *14*, 370.
- (18) Mildner, D. F. R. *Macromolecules* **1983**, *16*, 1760.
- (19) MacKnight, W. J.; Taggard, W. P.; Stein, R. S. *J. Polym. Sci., Polym. Symp.* **1974**, *45*, 113.
- (20) Tang, S. H. K. Ph.D. Thesis, The University of Akron, 1981.
- (21) Boue, F.; Nierlich, M.; Jannink, G.; Ball, R. *J. Phys. (Les Ulis, Fr.)* **1982**, *43*, 137.
- (22) Hadziioannou, G.; Wang, L. H.; Stein, R. S.; Porter, R. S. *Macromolecules* **1982**, *15*, 880.